

C D J Emin and J F Werner

GEC Research Laboratories  
Hirst Research Centre  
Wembley UK

**BEST  
AVAILABLE COPY**

ABSTRACT

Lithium tetraborate is a new piezoelectric material which has been shown to have improved properties for SAW applications. In view of this the bulk acoustic wave properties have been predicted for both singly and doubly rotated cuts, using the values of the material constants and their temperature coefficients currently available.

One of the orientations investigated showed potentially interesting properties. An  $X_2$ -cut rotated  $56^\circ 40'$  about  $X_1$  displayed a zero room temperature first order temperature coefficient of frequency for the thickness shear mode. Although there is strong coupling to a thickness extensional mode this is well separated out in frequency and the response is effectively single moded.

The piezoelectric coupling constant for the thickness shear mode was predicted to be greater than 6%, comparing favourably with AT quartz (0.8%) and  $28^\circ$  rotated berlinite (3%).

Preliminary measurements on single resonator devices have been conducted. The existence of a parabolic frequency/temperature performance has been confirmed with second order temperature coefficient of  $30 \times 10^{-8} \text{C}^{-2}$ . Although the turnover temperature shows a tendency to shift with the value of  $\lambda/t$  (where  $\lambda$  is the electrode length and  $t$  the resonator thickness) devices have been designed with a room temperature turnover and a variation of  $\pm 50$  ppm between 0 and  $40^\circ\text{C}$ . Although this is higher than AT quartz ( $\pm 0.5$  ppm) the capacitance ratio of these devices has been measured as low as 20 compared with a value for AT quartz in excess of 200.

The maximum attainable bandwidth of a filter using quartz bulk mode resonators is 1%, achieved using complicated synthesis and optimisation techniques. Simple lithium borate bulk wave filters should have fractional bandwidths significantly wider than this and it is expected that by using design techniques similar to those used for quartz filters further improvements could be made.

INTRODUCTION

There is an increasing demand in signal processing systems for compact electronic components using surface acoustic waves (SAW) or bulk acoustic waves (BAW) in piezoelectric substrates. These components include filters, delay lines, encoders, decoders and correlators. The most commonly used substrate material has been  $\alpha$ -quartz which offers good mechanical and chemical stability, high intrinsic Q and single rotated cuts with a zero first order temperature coefficient of frequency (TCF) for both SAW and BAW applications.

Unfortunately quartz exhibits weak electromechanical (EM) coupling which is a limiting factor in achieving certain device specifications such as bandwidth and insertion loss. Over certain frequency ranges SAW

transversal filters and BAW resonator filters provide roughly complementary technologies. However there are significant applications in modern radar and communication systems, which require frequency selectivities difficult to achieve with SAW's, combined with bandwidths impracticable for BAW crystal filters. With AT quartz resonators a fractional bandwidth of 1% is feasible but in this region the effects of losses in inductors which are essential to the design are very significant. These problems can be overcome by sophisticated synthesis and optimisation techniques but there is an inevitable practical penalty in terms of sensitivity and ease of construction. There exists, therefore, an urgent need for a material with both high EM coupling and zero first order frequency temperature coefficient.

Materials that have been investigated in recent years include lithium niobate, lithium tantalate and aluminium phosphate (berlinite). Table 1 shows the EM coupling

Material and cut	EM coupling k	k <sup>2</sup>	Minimum effective C <sub>0</sub> /C <sub>1</sub>	Maximum bandwidth %
Lithium niobate $163^\circ X_2$	0.615	0.378	8	12.5
Lithium tantalate $163^\circ X_2$	0.408	0.166	17	6
Lithium tetraborate $56^\circ 40' X_2$	0.281	0.0792	20*	5
Berlinite $28^\circ X_2$	0.15	0.0225	90	1.1
Quartz (AT)	0.089	0.00792	250	0.4

(a) Fundamental mode

Lithium niobate $163^\circ X_2$	0.615	0.042	70	1.4
Lithium tantalate $163^\circ X_2$	0.408	0.0184	170	0.6
Lithium tetraborate $56^\circ 40' X_2$	0.281	0.0088	380*	0.26
Berlinite $28^\circ X_2$	0.15	0.0025	800	0.12
Quartz (AT)	0.089	0.00088	2000	0.05

(b) Third overtone \* Experimentally determined values

Table 1 Comparison of filter performance

AD P 002465

factors and maximum bandwidths of these materials for fundamental and third overtone mode operation. However attempts to build useful filters with these materials have unearthed a number of complications.

Lithium niobate and lithium tantalate exhibit trigonal symmetry with point group  $3m$ , and for both materials there exists, in addition to the major axes, a pseudo-threefold axis rotated  $163^\circ$  from  $+X_2$  about  $X_1$  (See Figure 1). A plate prepared at this rotation has a vibrational mode structure similar to AT quartz, but the TCF is of the order of  $-80 \text{ ppm}/^\circ\text{C}$  for lithium niobate, and  $-20 \text{ ppm}/^\circ\text{C}$  for lithium tantalate. A double rotated ( $\alpha=75^\circ$ ,  $\beta=14^\circ$ ) plate of lithium tantalate has a zero TCF at  $25^\circ\text{C}$ , but it has been found that the mode spectrum of resonators operating at fundamental mode for this orientation is distorted by high overtone flexural modes moving through the main response with a TCF of  $-50 \text{ ppm}/^\circ\text{C}$ . The TCF for operation at third overtone is  $-40 \text{ ppm}/^\circ\text{C}$ .

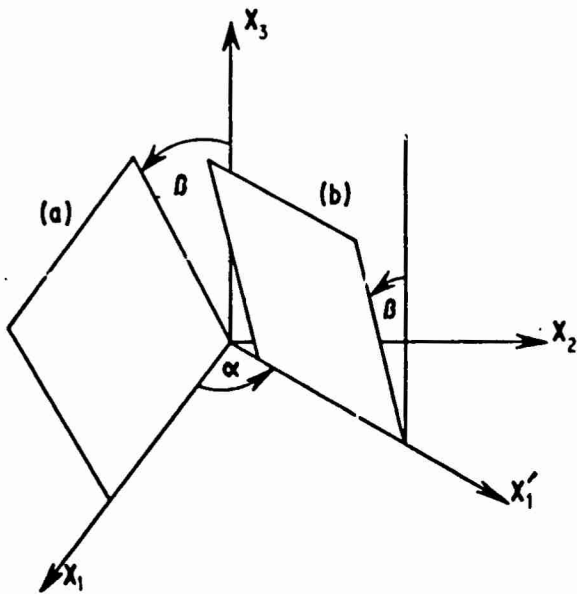


Figure 1 Conventions for specifying plate rotations with respect to crystal axes  $X_1, X_2, X_3$   
(a) Single rotation  $\beta$  (b) Double rotation  $\alpha\beta$

More recently berlinite has been examined as a possible substrate material<sup>2,3</sup>. Berlinite is isomorphic with quartz and has a  $28^\circ X_2$  plate analogous to the AT cut in quartz. Work performed at Hirst Research Centre on berlinite bulk wave resonators has demonstrated a cubic frequency temperature performance with turnovers at room temperature and  $100^\circ\text{C}$ . However berlinite offers only a marginal improvement in EM coupling, and berlinite resonators exhibit many undesirable features such as an hysteresis effect on temperature cycling and very low Q values. This was almost certainly due to the fact that the best quality material available had a water content of as much as 1 mg/g in  $X_2$  axis grown material<sup>4</sup>. Growth of single crystal boules by hydrothermal synthesis has proved difficult not least because of its reverse solubility, and investigation of this material has subsequently been discontinued.

Lithium tetraborate ( $\text{Li}_2\text{B}_4\text{O}_7$ ) is a new material which has been arousing interest for possible SAW applications<sup>5</sup>. It was chosen initially in the hope

that its low density ( $2451 \text{ kg/m}^3$ ) would result in high acoustic velocities. Single crystal boules have been grown using the Czochralski technique<sup>6,7</sup> and its symmetry has been determined as tetragonal 4mm. The elastic, dielectric and piezoelectric coefficients have been measured along with their first order temperature coefficients<sup>5</sup> and these have been used to calculate BAW properties for single and double rotations of lithium tetraborate plates.

#### THEORY OF THICKNESS MODE PLATE VIBRATORS

The first exact solution to the problem of vibrations in piezoelectric plates with wave propagation in the thickness direction only was due to Tiersten<sup>8</sup>. He considered the case of an homogenous, anisotropic, infinite plate with infinite massless electrodes subjected to an alternating potential difference. The faces of the plate are assumed to be traction free with  $X_1$  arbitrarily selected as the plate normal. No  $X_2$  or  $X_3$  dependence is assumed. The analysis proceeds in the following stages.

(i) The rotated material constants are obtained for a particular orientation using relations of the form

$$C'_{ijkl} = \sum_{rstu} V_{1r}V_{1s}V_{1t}V_{1u} C_{rstu} \quad (1)$$

where  $V_{ij}$  is the rotation matrix and  $C'_{ijkl}$  corresponds to the rotated elastic constant matrix. In the following text  $C_{ijkl}$ ,  $e_{ijk}$ ,  $\epsilon_{ij}$  are used to represent the rotated values of the elastic, piezoelectric and dielectric constants.

(ii) The stiffened elastic constants  $\bar{C}$  are computed using the relation

$$\bar{C}_{ijkl} = C_{ijkl} + \frac{e_{11j}e_{11k}}{\epsilon_{11}} \quad (2)$$

(iii) Following Tiersten, solutions of the stress equations of motion including piezoelectric stiffening have been assumed to take the form  $U_j = A_j \sin n X_1$ . This requires

$$(\bar{C}_{ijkl} - C\delta_{jk}) A_k = 0 \quad (3)$$

where  $\delta_{jk}$  is the Kronecker  $\delta$ . This matrix equation is solved by Householder reduction<sup>9</sup> yielding three real positive roots  $C^{(1)}$  corresponding to the acoustic velocity of three modes a, b and c. Mode a is therefore a thickness extensional mode whilst b and c are the fast and slow thickness shear modes. Each mode has an associated eigenvector  $A_k^{(1)}$  corresponding to the polarisation of the particle displacement.

(iv) The EM coupling factor  $K_{(1)}^2$  is defined as

$$K_{(1)}^2 = \frac{\left( \sum_k A_k^{(1)} e_{11k} \right)^2}{\left( \sum_k A_k^{(1)2} \right) C^{(1)} \epsilon_{11}} \quad (4)$$

and is plotted in Figure 2 as a function of  $\beta$  for each of the three modes where  $\beta$  corresponds to an orientation from  $+X_2$  about  $X_1$ .

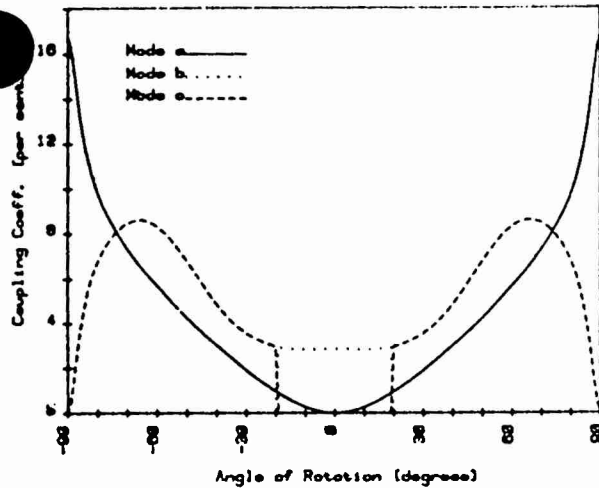


Figure 2 Coupling coefficient as a function of angle of rotation  $\beta$ . Fundamental mode

(v) The natural resonances and antiresonances of the plate are obtained from the poles and zeros of the input admittance<sup>10</sup>. These occur at

$$1 - \sum_i k^2(i) \frac{\tan Y(i)}{Y(i)} = 0 \text{ for antiresonance (5)}$$

$$1 - \sum_i k^2(i) \frac{\tan Y(i)}{Y(i)} = 0 \text{ for resonance (6)}$$

If the plate faces occur at  $Y_i = \pm h$  then  $Y(i) = h\eta(i)$ . Equation (5) is simply satisfied for  $Y(i) = m\pi/2$  for  $m$  odd yielding an infinite set of harmonically related antiresonant frequencies  $f_a$ . Equation (6) has three series of coupled roots. For single rotations of  $\text{Li}_2\text{B}_4\text{O}_7$  only two modes are excited simultaneously and for simplicity it is assumed that these modes are uncoupled. This is a reasonable assumption for certain values of the ratio of antiresonances for the two excited modes.

(vi) Values of the frequency constants are computed by an iterative solution of the equation

$$Y(i) = \arctan \left[ \frac{n\pi}{2} \frac{f_r(n)}{f_a(n)} \frac{1}{k^2(i)} \right] \quad (7)$$

(with  $n=1$  for the fundamental mode and  $n=3$  for the third overtone mode) using the relations

$$Y(i) = \frac{n\pi}{2} \frac{f_r(n)}{f_a(n)} \text{ and } f_a(n) = \frac{n}{4} \frac{V(i)}{h}$$

the piezoelectrically stiffened phase velocities  $\left(\frac{C(i)}{\rho}\right)$ . Frequency constants for the three modes are plotted as a function of  $\beta$  in Figure 3.

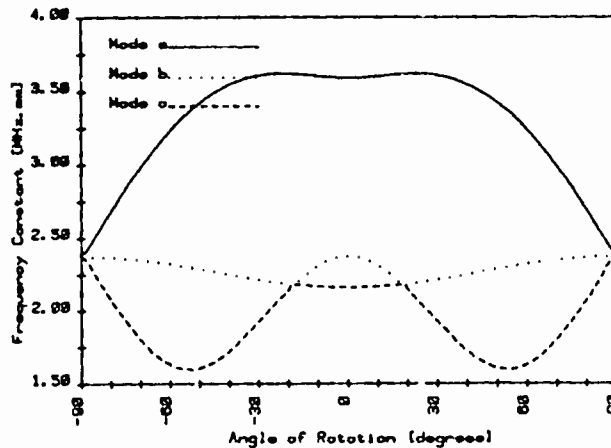


Figure 3 Frequency constant as a function of rotation angle  $\beta$ . Fundamental mode

(vii) Finally the resonant frequencies are adjusted for temperature by using the temperature coefficients of the material constants and their thermal expansion coefficients (see Table 2). The resonant frequencies are computed at room temperature  $\pm 0.5^\circ\text{C}$  and a TCF is calculated from the slope obtained from these points.

Coefficient	Magnitude	Temperature coefficient ( $10^{-6}^\circ\text{C}^{-1}$ )
$C_{11}$	12.67	-125
$C_{12}$	0.05	14000
$C_{13}$	3.0	350
$C_{33}$	5.39	354
$C_{44}$	5.50	-23
$C_{66}$	4.60	-480
$e_{15}$	0.36	-1300
$e_{31}$	0.19	-1300
$e_{33}$	0.89	-1000
$\epsilon^s_{11}$	8.97	-110
$\epsilon^s_{33}$	8.15	-33
$a_{11}$	13.0	
$a_{33}$	-1.5	

Table 2 Elastic stiffness ( $10^{10} \text{ Nm}^{-2}$ ) piezoelectric ( $\text{cm}^{-2}$ ) and relative dielectric constants and their first order temperature coefficient at  $20^\circ\text{C}$ . These were the values used in the calculations. [From Shorrocks et al 1982].  $a_{11}$  and  $a_{23}$  are the linear expansion coefficients ( $10^{-6} \text{ m}^\circ\text{C}^{-1}$ )

These are plotted in Figure 4 for the fundamental mode and Figure 5 for the third overtone mode. It is clear from Figures 2 and 4 that there exists single orientations of  $\text{Li}_2\text{B}_4\text{O}_7$  plates for which there are zero TCF's for both the electrically excited modes. These occur at  $\beta = \pm 38^\circ 49'$  (thickness extensional) and  $\pm 48^\circ 48'$  (thickness shear) for the fundamental mode,  $\pm 71^\circ 52'$  and  $\pm 68^\circ 17'$  for third overtone.

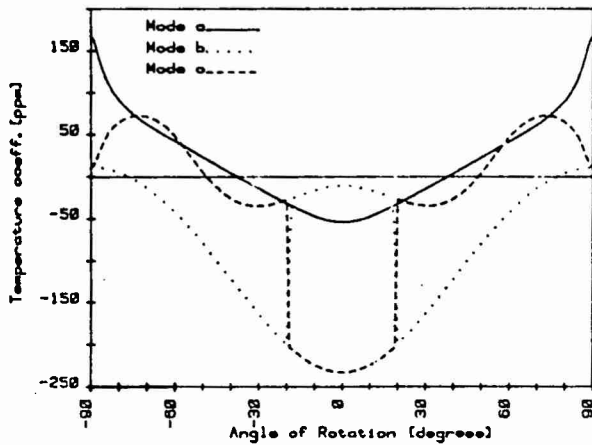


Figure 4 Temperature coefficient of frequency as a function of rotation angle  $\beta$ . Fundamental mode

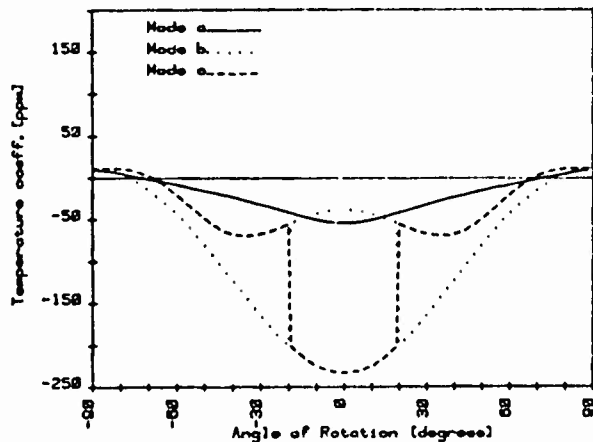


Figure 5 Temperature coefficient of frequency as a function of rotation angle  $\beta$ . Third overtone mode

The experimental data described below was obtained from lithium tetraborate resonators manufactured on plates cut at  $\beta = 56^\circ 40'$ , an orientation obtained from calculations based on earlier data. It has therefore been necessary to adjust all predictions to this orientation. The  $56^\circ 40'$  plate does in fact demonstrate a room temperature turnover for a given value of  $\lambda/t$  where  $\lambda$  is the electrode length and  $t$  the resonator thickness. In the case of infinite electrodes where  $\lambda/t \rightarrow \infty$  the turnover temperature for this plate tends to an upper limiting value well away from room temperature as anticipated. (see Figure 6).

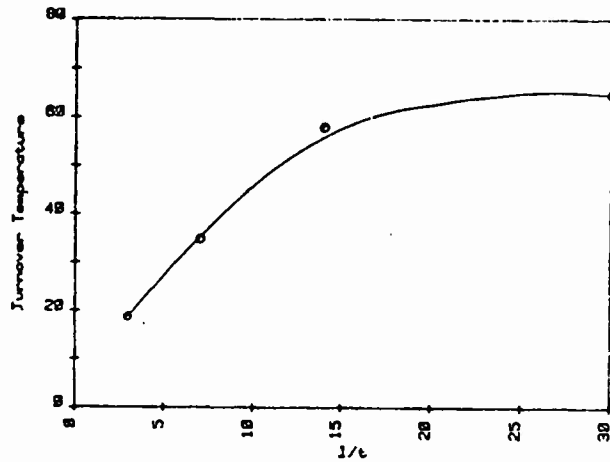


Figure 6 Turnover temperature as a function of electrode size

#### MATERIAL CHARACTERISATION AND DEVICE PREPARATION

The resonators used in these experiments were prepared with material obtained from an  $X_1$  axis grown crystal boules<sup>11</sup>. Optical examination revealed an annular core of defective material but away from the central region there were large areas of crystal that were relatively defect free.  $56^\circ 40'$  rotated  $X_2$  plates  $\sim 0.5$  mm thick were cut from the boules and then syton polished on both sides. The plates were checked for orientation by X-ray reflection and then the bulk of the material was examined using a Schlieren imaging technique. Circular blanks 8 mm in diameter were trepanned from the best material and then reduced to  $\sim 0.1$  mm thickness using a stretched carrier lapping machine. A final inspection of the blanks by the Haidinger fringe method revealed a thickness uniformity of 1 part in  $10^3$ .

Blank characterisation proceeded by measuring the blank frequencies at 3rd and 5th overtone in 6 mm diameter air-gap electrodes. Together with a measurement of the thickness using a digital micrometer a value of the frequency constant for the unplated blank was obtained. This was found to be  $1700 \pm 50$  kHz mm.

#### SINGLE RESONATOR DESIGN

In order to design a single resonator it is necessary to extend the mathematical treatment to allow for the effect of finite electrodes with finite mass. Such a treatment based on a wave propagation analysis for integrated filters has been used previously for the design of AT quartz resonators<sup>12</sup> and an adaptation of this technique has proved successful in predicting the properties of resonators manufactured from higher coupling materials such as  $163^\circ$  rotated  $X_2$  lithium tantalate. As a first approximation this technique has been used for  $56^\circ 40'$  rotated  $X_2$  lithium tetraborate. The method involves treating the electroded and unelectroded regions as having the same thickness,  $t$ , but separate densities  $\rho_E$  and  $\rho_U$ <sup>13</sup>. Solutions are obtained for standing waves in the electroded region and an evanescent wave in the surrounding region; the solutions being matched across the boundary. For square electrodes of length  $\lambda$  these solutions depend on the ratio  $\lambda/t$ , corresponding to the Bechmann conditions for quartz.

The information required is the rotated elastic, piezoelectric and dielectric constants and an estimate of the intrinsic Q of the material. The value used was  $10^6$  at 1 MHz by measuring the Q of a device at 7th overtone and extrapolating back (Figure 7). Thus values of the fractional mass loading, (defined as  $\mu-1$  where  $\mu = \mu^2/\rho u$ ) and resonator Q have been calculated as functions of plateback for the fundamental and third overtone modes. Here plateback is defined as  $(f_u - f_p)/f_u$ .  $f_u$  is the resonant frequency of the blank and  $f_p$  the frequency after plating. These are illustrated in Figures 8 to 11 for a range of values of  $l/t$  and were used as the design criteria for energy trapped resonators.

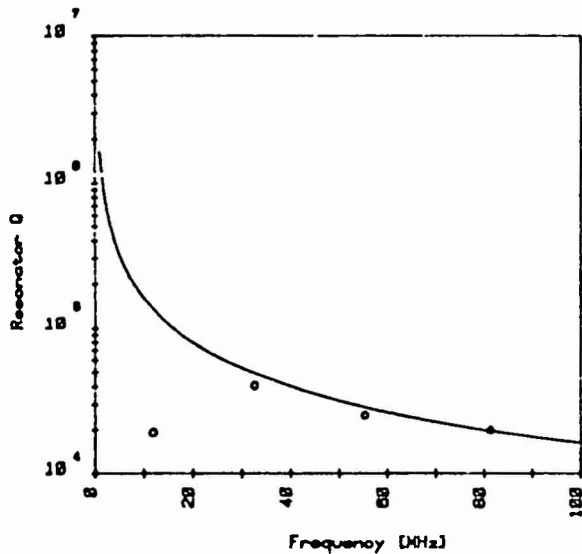


Figure 7 Intrinsic Q as a function of frequency.  
 — Extrapolated from resonator Q at third overtone  
 o Experimental value for 1,3 and 5

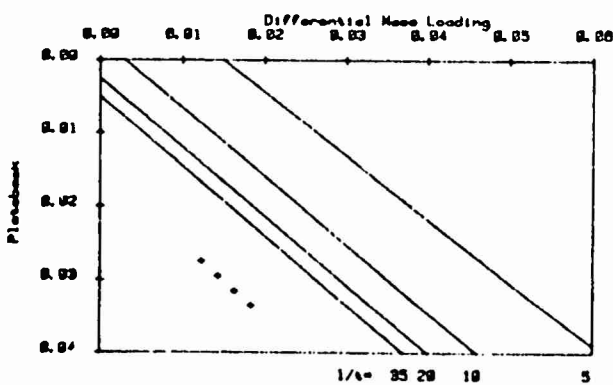


Figure 8 Differential mass loading as a function of plateback for the fundamental mode  
 — Theory  
 + Experiment ( $l/t=14$ )

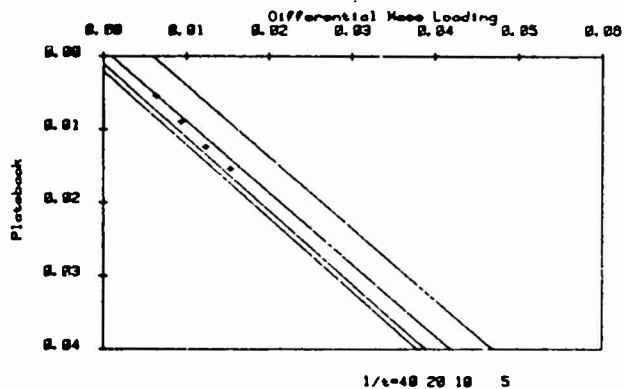


Figure 9 Differential mass loading as a function of plateback for the third overtone mode  
 — Theory  
 + Experiment ( $l/t=14$ )

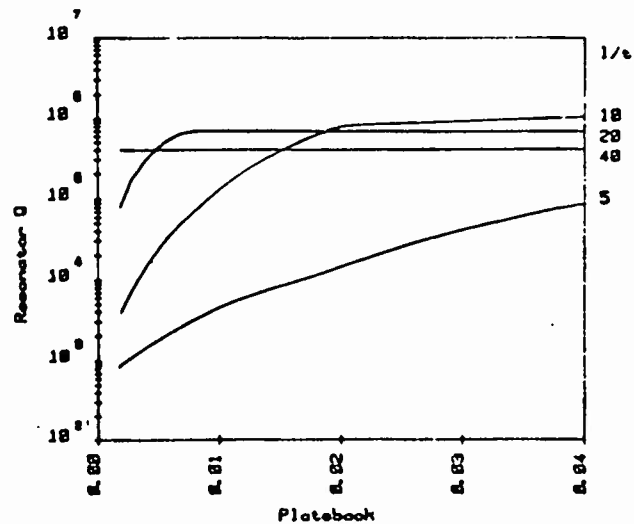


Figure 10 Plot of plateback/resonator Q for the fundamental mode

#### EXPERIMENTAL RESULTS

Groups of lithium tetraborate resonators have been fabricated with values of  $l/t$  from 3 to 30. The crystal equivalent circuit parameters and frequency temperature characteristics of these devices have been examined.

#### EQUIVALENT CIRCUIT PARAMETERS

The equivalent circuit parameters of the lithium tetraborate resonators have been determined using an automated measurement technique previously described for the measurement of quartz resonators<sup>14</sup>. The four S-parameters of the device are measured (transmission measurement), then error corrected using a standard 12

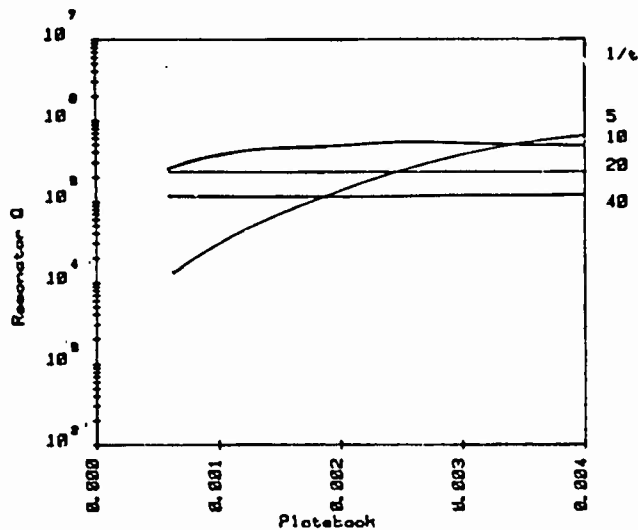


Figure 11 Plot of plateback/resonator Q for the third overtone mode

term error model and finally a non-linear least squares fit is performed using the transmission coefficient,  $S_{21}$ . A set of starting values is obtained from an initial survey of the measurements around series resonance which are iteratively refined to obtain optimum values of the crystal parameters R, L, C and  $C_0$ . The measured and calculated responses are then displayed. Figures 12 and 13 show typical outputs for the fundamental and third overtone mode. Accurate, repeatable measurements of crystal parameters can be obtained in this way with traceability to the precision 50 ohm components used in the calibration procedure. A comparison between the values of the measured parameters and those predicted by the single resonator design program is shown in Table 3. The experimental values quoted are averaged over eight resonators. These results are discussed below.

Freq (MHz)	$C_0$ (pF)	ESR	$L_m$ (mH)	$C_m$ (pF)	Q
11.6586487	1.10	39.0	4.85	$3.841E-02$	5965

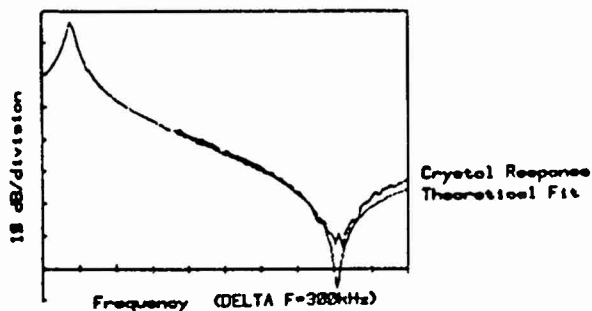


Figure 12 Typical response of a fundamental mode crystal resonator, together with the best value parameter fit

Freq (MHz)	$C_0$ (pF)	ESR	$L_m$ (mH)	$C_m$ (pF)	Q
33.3821785	1.14	275.53	60.68	$3.425E-04$	51698

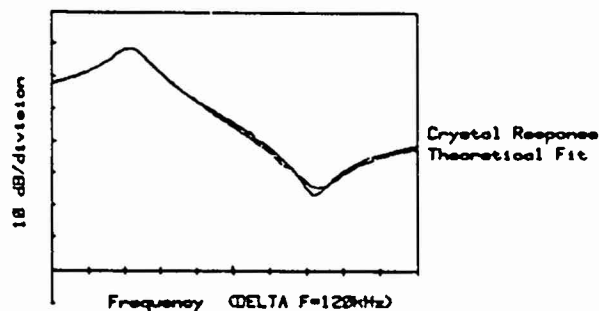


Figure 13 Typical response of a third overtone mode crystal resonator, together with the best value parameter fit

#### FREQUENCY TEMPERATURE BEHAVIOUR

The variation of resonant frequency with temperature has been investigated in two separate ways.

In order to examine the existence of a room temperature zero TCF, an environmental chamber equipped with both heating elements and  $CO_2$  cooling was used to provide ambient temperature from  $-20^\circ C$  to  $80^\circ C$ . Accurate measurements of temperature were made by encapsulating the resonators and then fastening platinum resistance sensors to the container. The frequency was monitored in two ways. Where possible an oscillator circuit was used incorporating a 12 MHz low pass filter to prevent frequency hopping to either the thickness extensional or higher overtone thickness shear responses. The frequency could then be read directly from a counter. Where this was not possible, due to high insertion losses or general lack of stability, frequencies were monitored directly on a spectrum analyser.

The measured data was stored on magnetic tape. Analysis of the data involved making a parabolic fit by the method of least squares. The results are summarised in Figure 14. It is clear from these results that there exists a first order zero TCF but that the turnover temperature is dependent on the value of  $l/t$ .

The frequency temperature characteristic of a resonator was measured over a wider temperature range, 4 K to 300 K, to look for possible coupling with other modes of vibration which could give rise to lower values of resonator Q. Automated acoustic loss and frequency measurements were made as a function of temperature using a helium/nitrogen flow cryostat system described previously<sup>15</sup>. A slightly modified form of the precision crystal parameter measurement technique was utilised. The frequency-temperature characteristic of the resonator is shown in Figure 15 as a percentage change relative to the frequency at 4 K. A large acoustic loss occurs in the 50-70 K temperature regime giving rise to the discontinuity in the frequency-temperature plot. Discontinuities in the range 85-105 K are indicative of coupled modes. A large acoustic loss peak at 160 K gives rise to the inflection in the characteristics in that region. Above about 100 K the main response appears unaffected by spurious modes.

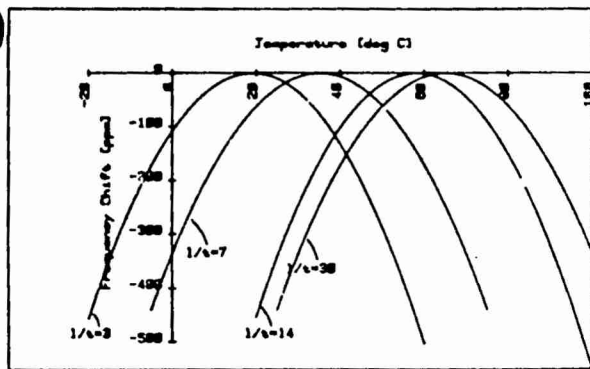


Figure 14 Frequency/temperature characteristics of lithium tetraborate resonators for different electrode sizes.  $F=11$  MHz

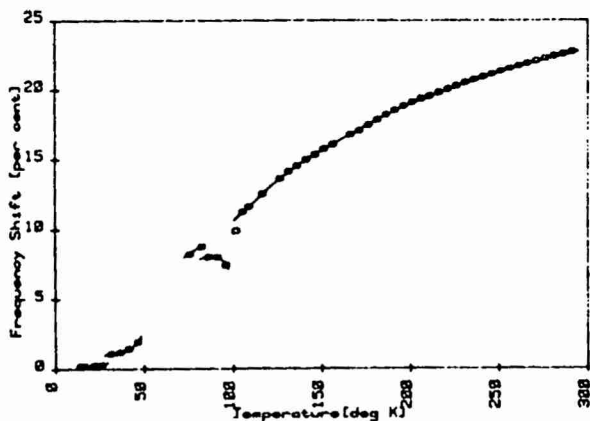


Figure 15 The frequency/temperature characteristics of a lithium tetraborate resonator from 4.2K to room temperature

### DISCUSSION

Theoretical calculations have shown a number of orientations of lithium tetraborate offer temperature stability and high electromechanical coupling. A study of the temperature performance of a  $56^{\circ}40$  Y rotated plate has revealed some interesting points. For values of  $l/t = 30$  the frequency/temperature behaviour is approximately linear with a positive slope of  $20$  ppm/ $^{\circ}C$  as expected. However experiment has shown that as  $l/t$  decreases the temperature for zero TCF decreases rapidly reaching  $20^{\circ}C$  for  $l/t = 3$ . It is also noted that an increase in turnover temperature with  $l/t$  has been achieved by replating the same resonator with different size electrodes. In addition it is independent of electrode orientation with respect to the face axes  $X_1$  and  $X_3$ . Furthermore, using the linear temperature coefficients available a minimum in the frequency/temperature curve is anticipated with a second order coefficient of  $+30 \cdot 10^{-9} C^{-2}$  (which is comparable to ST quartz) whereas in practice a maximum has been obtained with a coefficient  $-300 \pm 50 \times 10^{-9} C^{-2}$ . It seems evident that the first order temperature coefficients are only accurate for  $25^{\circ} \pm 5^{\circ}C$  and particularly for temperatures in excess of  $30^{\circ}$  higher order terms are required.

Measurements of the electrical parameters of single resonators have shown a number of interesting properties; the most striking being the large anomalies between predicted and theoretical values for fundamental responses whilst at third overtone far better agreement has been obtained (see Table 3). This would seem to point to cross-coupling between the fundamental mode and some other mode: the only other electrically excited being a thickness extensional mode with a frequency constant more than double that of the fundamental shear mode. Electrical coupling to this mode ( $k^2 = 4\%$ ) cannot explain the increase in coupling required to account for the anomalously high platebacks shown in Figure 8.

The measured Q values for the fundamental mode are an order of magnitude less than anticipated although good agreement has been shown for higher overtone modes.

Measured values														Predicted		
Mode	Frequency	Electrode size	$l/t$	Frequency constant	Plateback	Static capacitance	Motional capacitance	Capacitance ratio	Motional inductance	esr	Q	Turnover temperature	2nd TCF	Motional inductance	esr	Q
	MHz	$mm^2$		$kHz/mm$		pF	$pF \cdot 10^{-2}$		mH	ohms		$^{\circ}C$	$10^{-9} C^{-2}$	mH	ohms	
1	10.56	0.5	3	1720	0.01	1.13	1.86	60	12.2	270	2970	19	-300			
1	11.65	1.0	7	1747	0.017	1.1	3.8	29	4.8	36	9700	35	-290	37.2	34	79200
3	33.3	1.0	7		0.008	1.4			66.6	270	51700			35.0	205	35000
1	11.10	2.0	14	1650	0.038	2.93	14.5	20	1.43	10	9091	58	-314			
1	11.19	4.5	30	1747	0.036	19.0	63.4	30	0.32	10	5500	65	-275			

Table 3 Summary of results obtained on lithium tetraborate resonators

This may be due to mechanical coupling resulting in damping of the fundamental mode or loss of energy through some flexural or thickness twist mode.

It is possible that some approximations in the one dimensional theory and the single resonator theory breakdown in the case of some high coupling materials. Recently a more general theory has solved the problem for coupled acoustic modes in partially contoured crystal resonators<sup>16</sup> and it is hoped to extend this to flat crystal blanks. Even while the fundamental mode behaviour is not fully understood it is still apparent that useful devices can be made on lithium tetraborate at both fundamental and third overtone.

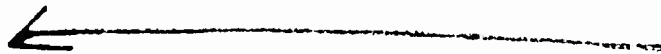
#### ACKNOWLEDGEMENT

The authors would like to thank Mr D Robertson of RSRE, Malvern for supplying the lithium tetraborate boules.

Part of this work has been carried out with the support of Procurement Executive, Ministry of Defence, sponsored by DCVD.

#### REFERENCES

- 1 J W Burgess, R J Porter, Procs 27th AFCS, 246, 1973
- 2 Z P Chang, G R Barsch, IEEE Transactions on Sonics and Ultrasonics, SU-23, 2, 127, 1976
- 3 J Detaint et al, Procs of the 34th AFCS, 93, 1980
- 4 M J Bevan, GEC Research Laboratories, Divisional Report, MS16431, 1982
- 5 N M Shorrocks et al, Procs. IEEE Ultrasonics Symposium, 337, 1981
- 6 S R Nagel et al, J. Amer. Ceram. Soc., 60 (3-4), 172, 1977
- 7 J D Garrett et al, J. Cryst. Growth., 41, 225, 1977
- 8 H F Tiersten, J. Acoust. Soc. Amer., 35, 53, 1963
- 9 A Ralston, P Rabinowitz, A first course in numerical analysis, p 511, 2nd Ed. McGraw-Hill, 1978
- 10 T Yamada, N Niizeki, Proc. IEEE, 58, 941, 1970
- 11 Supplied by D Robertson, RSRE, Malvern
- 12 J F Werner, A J Dyer, Procs 30th AFCS, 40, 1976
- 13 W Shockley et al, Procs 17th AFCS, 88, 1963
- 14 R C Peach et al, Procs 36th AFCS, 297, 1982
- 15 S P Doherty et al, Procs 36th AFCS, 66, 1982
- 16 R C Peach, Procs 36th AFCS, 22, 1982





END

DATE  
FILMED

2 - 84

DTIC